Applied Catalysis B: Environmental 321 (2023) 122027

Contents lists available at ScienceDirect

Applied Catalysis B: Environmental

journal homepage: www.elsevier.com/locate/apcatb

High selectivity toward CO evolution for the photocatalytic conversion of CO_2 by H_2O as an electron donor over Ag-loaded β-Ga_2O_3

Xuanwen Xu [a], Tsunehiro Tanaka [a,b], Kentaro Teramura [a,b,*]

[a] Department of Molecular Engineering, Graduate School of Engineering, Kyoto University, Kyotodaigaku Katsura, Nishikyo-ku, Kyoto 615−8510, Japan
[b] Elements Strategy Initiative for Catalysts & Batteries (ESICB), Kyoto University, 1−30 Goryo-Ohara, Nishikyo-ku, Kyoto 615−8245, Japan

ARTICLE INFO

Keywords:
Selectivity
CO
ORR
Gallium oxide
Ag

ABSTRACT

In this work, the performances of Ag-loaded commercial Ga_2O_3 (composite of α- and β-Ga_2O_3), pure α-, and β-Ga_2O_3 were examined for the photocatalytic conversion of CO_2 by H_2O. Ag-loaded β-Ga_2O_3 exhibited high selectivity for CO evolution if the proper loading methods and Ag nanoparticle contents were controlled. Using the chemical reduction method with NaH_2PO_2, 2 wt% Ag nanoparticles on β-Ga_2O_3 produced CO with an activity of 201.3 μmol h^{-1} and selectivity of 83.5%. However, 8 wt% Ag nanoparticles were required to achieve the same selectivity when prepared using the photodeposition method. By varying the amount of Ag-loaded β-Ga_2O_3 for the reaction, it was found that the selectivity toward CO evolution was largely dependent on the amounts of Ag-loaded β-Ga_2O_3. The active sites where H_2 molecules are formed are poisoned by the oxygen reduction reaction (ORR) at high amounts of Ag-loaded β-Ga_2O_3, resulting in a high selectivity for CO evolution.

1. Introduction

The emission of greenhouse gases [1], mainly carbon dioxide (CO_2), has enhanced the effect of global warming [2] over the past 100 years. To reduce the CO_2 emission, various technologies for renewable energy [3] have been developed to replace fossil fuels. Among these alternative strategies, the utilization of solar energy [4] has attracted considerable attention owing to its sustainable and environmentally-friendly characteristics. This field can be divided into two branches from the perspective of energy conversion pathways: from solar to electricity directly, exemplified by silicon cells [5] and photovoltaic cells [6], and chemical pathways involving the conversion of biomass [7], water (H_2O) splitting [8], and CO_2 photoreduction [9]. Recently, the photocatalytic conversion of CO_2 using H_2O as the electron donor has been achieved over many photocatalysts including Ag-loaded $NaTaO_3$ [10], $CaTiO_3$ [11], Ga_2O_3 [12], and $ZnGa_2O_4$ [13] among others.

Many studies have revealed that bare Ga_2O_3 exhibits low selectivity toward the evolution of CO during the photocatalytic conversion of CO_2 by H_2O when only Ag nanoparticles are used as a cocatalyst. Kawaguchi et al. [14] compared the performances of commercial and homemade Ga_2O_3 modified with Ag nanoparticles for the photocatalytic conversion of CO_2 using H_2O. Their results showed that CO evolution selectivity failed to exceed 40%, regardless of loading method. Li et al. [15] achieved a selectivity of 65.3% for the formation of CO on Ni-doped β-Ga_2O_3 modified by Ag nanoparticles. However, the CO production activity was quite low. Previously [12,16–18], a similar level of selectivity toward the evolution of CO over Ag-loaded Ga_2O_3 (29.9–51.0%) for the photocatalytic conversion of CO_2 by H_2O was achieved by our group. In contrast, modifications of Zn species [19,20] as well as rare earth elements such as Pr and Ce [16,17] on Ga_2O_3 were shown to enhance the selectivity toward CO evolution (>80%) with Ag nanoparticles as the cocatalyst. In addition, a shell of $Cr(OH)_3$ covering the surface of Ag-loaded Ga_2O_3 promoted the selectivity for CO evolution (83%) during the photocatalytic conversion of CO_2 by H_2O [12]. Given these phenomena, it is possible that the selectivity for CO evolution over Ag-loaded Ga_2O_3 during the photocatalytic conversion of CO_2 by H_2O is largely dependent on the surface properties of Ga_2O_3. Herein, the performances of Ag-loaded commercial Ga_2O_3 (containing α and β phases) and homemade pure α- and β-Ga_2O_3 were examined for the photocatalytic conversion of CO_2 using H_2O. High selectivity toward CO evolution was achieved over Ga_2O_3 even though only Ag nanoparticles were used as the cocatalyst by controlling the loading extent and methods of the Ag nanoparticles. In addition, the selectivity was significantly affected by the phases of Ga_2O_3.

* Corresponding author at: Department of Molecular Engineering, Graduate School of Engineering, Kyoto University, Kyotodaigaku Katsura, Nishikyo-ku, Kyoto 615−8510, Japan.
E-mail address: teramura.kentaro.7r@kyoto-u.ac.jp (K. Teramura).

https://doi.org/10.1016/j.apcatb.2022.122027
Received 2 August 2022; Received in revised form 24 September 2022; Accepted 27 September 2022
Available online 29 September 2022

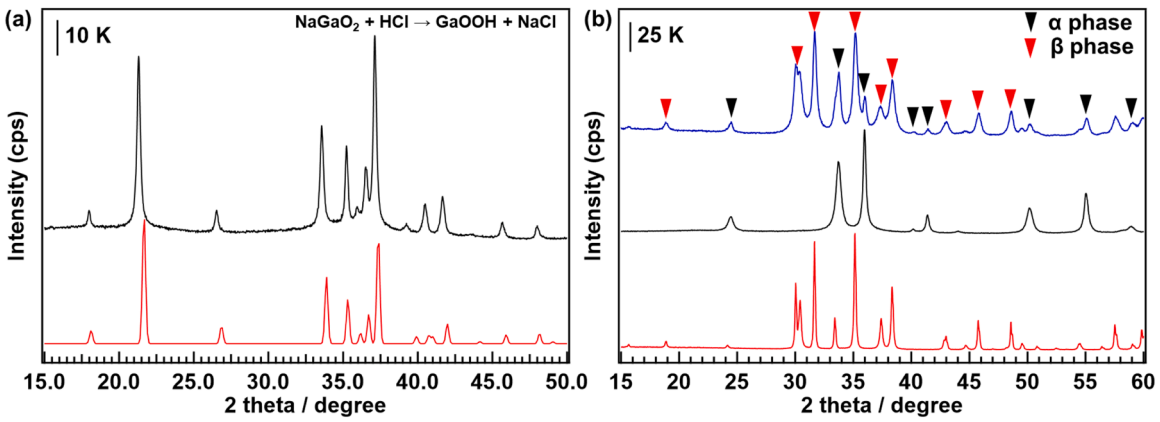

Fig. 1. XRD patterns of (a) synthesized GaOOH (black) and reference from ISCD database (red); (b) c-Ga_2O_3 (blue), α-Ga_2O_3 (black), and β-Ga_2O_3 (red).

2. Experimental

2.1. Photocatalyst preparation

Commercial Ga_2O_3 (c-Ga_2O_3) was purchased from KOJUNDO CHEMICAL LABORARTORY Co., Ltd. For the synthesis of α-Ga_2O_3, GaOOH was first fabricated by protonation of $NaGaO_2$ by HCl. The obtained GaOOH was dried at 358 K and washed at 358 K for 1 h. After drying, the powder was calcined at 723 K for 3 h. The β-Ga_2O_3 was obtained by calcinating commercial powder at 1423 K for 24 h in an aluminum crucible. The Ag nanoparticles were loaded into the above photocatalysts by various methods, including photodeposition, impregnation, and chemical reduction. The loading conditions are described in detail in Section S1.

2.2. Photocatalyst characterization

The structures of the obtained Ga_2O_3 used herein were determined using a Rigaku Ultima IV powder diffractometer (Cu Kα, 40 kV, and 40 mA). The morphologies of the photocatalysts were observed using a field-emission scanning electron microscope (FE-SEM, SU-8220, Hitachi High-Technologies). UV–vis diffuse reflectance spectroscopy (UV–vis DRS) of the photocatalysts was performed using a JASCO V-670 spectrometer. An X-ray fluorescence spectroscopy (XRF, EDX-8000, Shimadzu Corp.) was used to determine the ratios of elements if necessary.

2.3. Reaction procedure

An inner irradiation reactor equipped with a quartz jacket (Scheme S1) was used for the photocatalytic conversion of CO_2 using H_2O. The reactor was connected to cooling water to maintain the temperature between 298 and 303 K during the reactions. The light source was a 400 W high pressure mercury lamp (Sen Lights Corp.). Before the reactions, the system was purged with CO_2 to remove any residual air. The production of H_2, O_2, and CO was detected using GC-8A (Shimadzu Corp) gas chromatographs with TCD and FID detectors. The possible liquid products produced in the reactions were confirmed by a High-performance liquid chromatography (JASCO, LC-Net II/ADC).

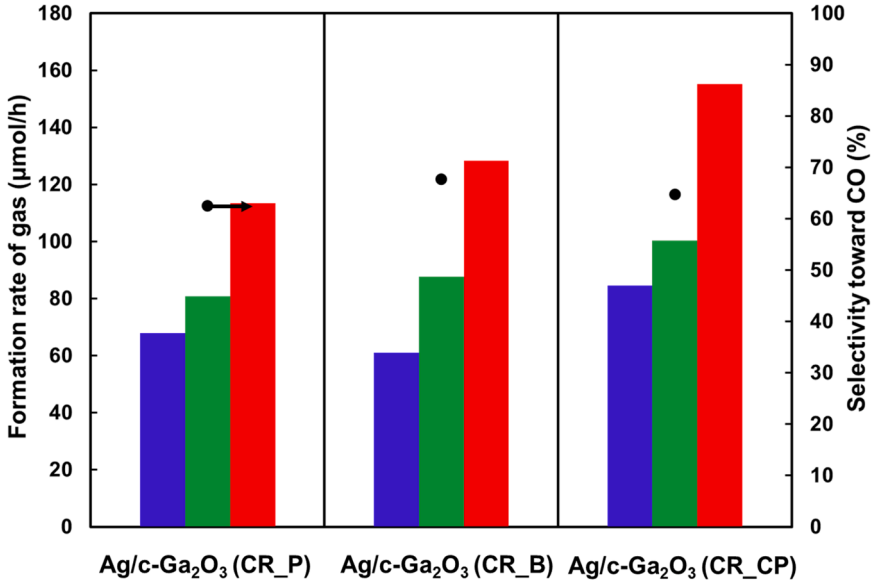

Fig. 2. Formation rates of H_2 (blue), O_2 (green), and CO (red) as well as selectivity toward CO evolution (black dots) for the photocatalytic conversion of CO_2 by H_2O over Ag/c-Ga_2O_3 (CR_P), Ag/c-Ga_2O_3 (CR_B), and Ag/c-Ga_2O_3 (CR_CP). Photoirradiation time: 0.5 h; Ag content: 2 wt%; photocatalyst loading: 0.25 g; reaction solution: 1.0 L of a 0.1 M $NaHCO_3$ aqueous solution; CO_2 flow rate: 30 mL min^{-1}; light
Source: a 400 W high-pressure Hg lamp.

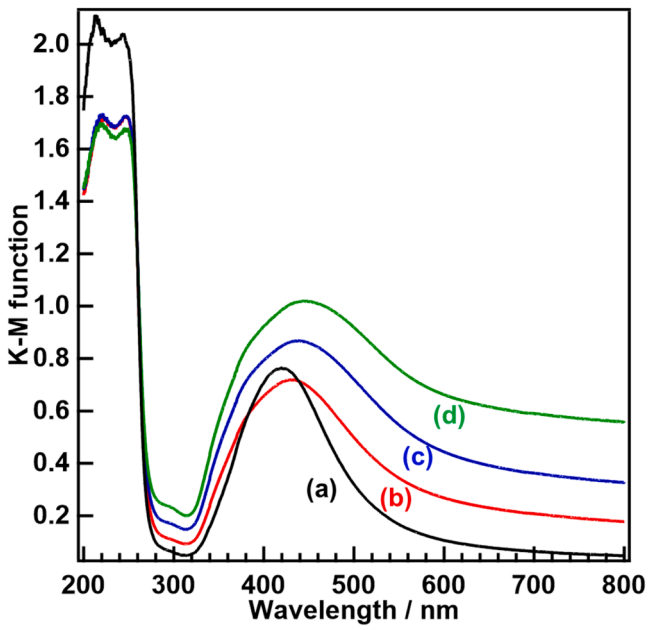

Fig. 3. UV–vis diffuse reflectance spectra of c-Ga_2O_3 with various Ag loadings by chemical reduction of NaH_2PO_2: (a) 1 wt%, (b) 2 wt%, (c) 3 wt%, and (4) 4 wt% Ag. The samples 2, 3 and 4 wt% Ag-loaded c-Ga_2O_3 were diluted by bare c-Ga_2O_3 before the measurements.

3. Results and discussion

3.1. Ag-loaded commercial Ga_2O_3

Fig. 1(a) shows the XRD patterns of the Ga-containing samples fabricated herein. The structure of GaOOH was successfully obtained by the protonation of $NaGaO_2$ by HCl. After calcination at 723 K, the GaOOH phase was converted to pure α-Ga_2O_3, as shown in Fig. 1(b). According to Fig. 1(b), c-Ga_2O_3 consisted of α- and β-Ga_2O_3 simultaneously, and pure β-Ga_2O_3 was obtained via calcination of c-Ga_2O_3 at 1423 K for 24 h. However, the half-width of the crystalline phase in α-Ga_2O_3 was visibly larger than that in β-Ga_2O_3, implying that the crystalline size of α-Ga_2O_3 was much smaller than that of β-Ga_2O_3.

Fig. 2 shows the photocatalytic performance of Ag-loaded c-Ga_2O_3 fabricated via chemical reduction by NaH_2PO_2 (Ag/c-Ga_2O_3 (CR_P)), $NaHBO_4$ (Ag/c-Ga_2O_3 (CR_B)), and a mixture of citric acid and NaH_2PO_2 (Ag/ c-Ga_2O_3 (CR_CP)) for the photocatalytic conversion of CO_2 by H_2O. A loading of 2 wt% Ag/c-Ga_2O_3 (CR_P) exhibited 62.5% selectivity (Eq. (1)) toward CO evolution during the photocatalytic conversion of CO_2 by H_2O, wherein CO and H_2 were formed at rates of 113.4 and 68.0 μmol h^{-1}, respectively. Note that $\boldsymbol{e^-/h^+}$ (Eq. (2)) during the reactions were very close to 1.0. On the other hand, there were no liquid products like HCOOH and CH_3OH being found in HPLC. Therefore, the other possible productions such as H_2O_2 [21] derived from the oxidation of H_2O should not be generated in the reactions. Although the formation rate of CO was slightly higher for Ag/c-Ga_2O_3 (CR_B) (128.4 μmol h^{-1}) and Ag/c-Ga_2O_3 (CR_CP) (155.3 μmol h^{-1}), the selectivity was similar (62.5–67.8%). Ag/c-Ga_2O_3 (CR_P) and (CR_CP) showed similar absorption properties and sizes of Ag nanoparticles (Fig. S1). Therefore, it is not confident to conclude that reduction reagents of mixture NaH_2PO_2 and citrate acid were obviously advantageous over NaH_2PO_2.

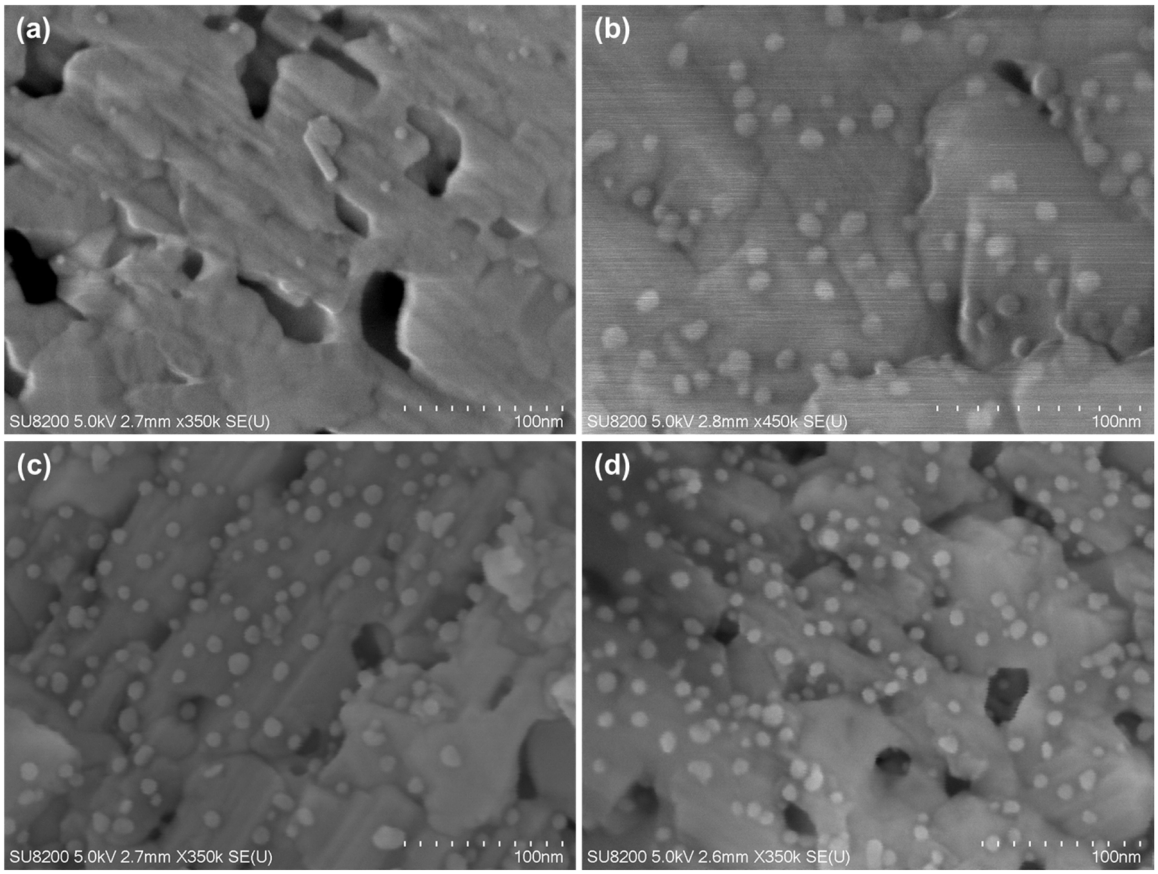

Fig. 4. SEM images of Ag/c-Ga_2O_3 (CR_P) at various loadings: (a) 1 wt%, (b) 2 wt%, (c) 3 wt%, and (d) 4 wt% Ag.

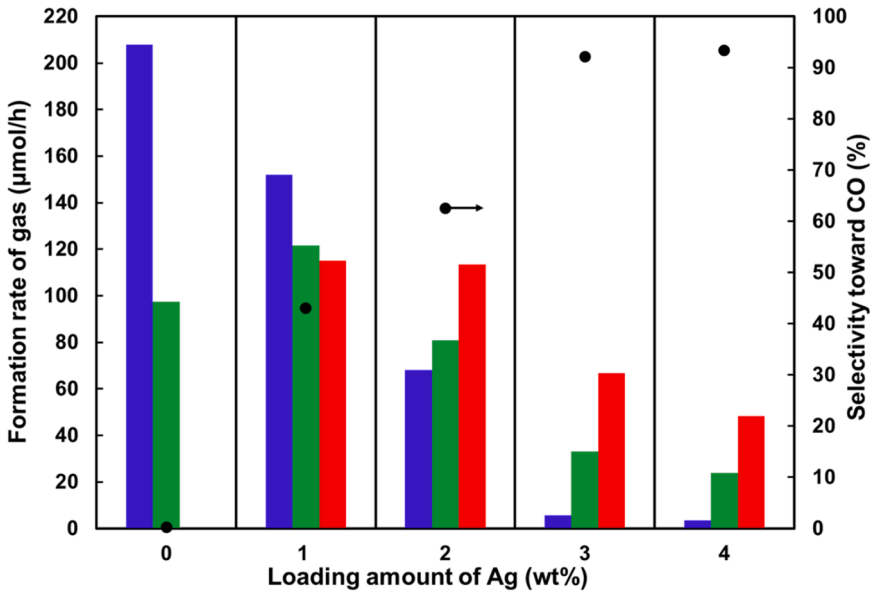

Fig. 5. Formation rates of H_2 (blue), O_2 (green), and CO (red) as well as selectivity toward CO evolution (black dots) for the photocatalytic conversion of CO_2 by H_2O over Ag/c-Ga_2O_3 (CR_P) with various Ag cocatalyst loadings. Photoirradiation time: 0.5 h; photocatalyst content: 0.25 g; reaction solution: 1.0 L of a 0.1 M $NaHCO_3$ aqueous solution; CO_2 flow rate: 30 mL min^{-1}; light
Source: a 400 W high-pressure Hg lamp.

$$\textbf{Selectivity} = R_{CO}/(R_{CO} + R_{H2}) \times 100\% \quad (1)$$

$$e^-/h^+ = (R_{CO} + R_{H2})/2R_{O2} \quad (2)$$

Fig. 3 shows the UV–vis diffuse reflectance spectra of c-Ga_2O_3 loaded with optimized amounts of Ag nanoparticles via chemical reduction with NaH_2PO_2. A clear surface plasmon resonance (SPR) absorption peak was observed at 420 nm for 1 wt% Ag nanoparticle loading (Fig. 3 (a)). With increased loading to 2 wt% Ag (Fig. 3(b)), the absorptive position red-shifted to 430 nm. For the loadings of 3 and 4 wt% Ag, the absorptive positions further shifted to 440 and 450 nm (Fig. 3(c) to (d)), respectively. On the other hand, it was found that the absorptive intensity dramatically increased when the loading of Ag reached 2 wt% (undiluted samples in Fig. S2). A shoulder absorption peak appeared at 290 nm, which was probably attributed to the transverse plasmon absorption band [22–24] of nonspherical Ag nanoparticles. Fig. 4 shows the SEM images of Ag-loaded c-Ga_2O_3 samples corresponding to those in Fig. 3. The Ag nanoparticle size was approximately 10 nm at 1 wt% loading and the coverage ratio of Ag nanoparticles on the surface of c-Ga_2O_3 was very low (Fig. 4(a)). As the loading was increased to 2 wt% (Fig. 4(b)), the near-elliptical Ag nanoparticles remained largely unchanged (approximately 10 nm). As shown in Fig. 4(c) and (d), 3 and 4 wt% Ag/c-Ga_2O_3 contained similarly sized Ag nanoparticles as in the 2 wt% Ag/c-Ga_2O_3 sample. This indicated that the red-shifts of absorptive positions observed in Fig. 3 were not caused by the sizes of Ag nanoparticles, even though it was previously reported that the absorption bands of metal nanoparticles depend on their sizes [25,26] to some degree. However, the coverage ratio of Ag nanoparticles on the surfaces of c-Ga_2O_3 visibly increased, resulting in Ag nanoparticles closed to each other. This indicates that the chemical reduction by NaH_2PO_2 changed the coverage ratio on the surface of c-Ga_2O_3 while maintaining the Ag nanoparticle size. The red-shifts of absorptive positions of Ag nanoparticles were probably caused by the strong coupling of surface plasmon resonance inter- nanoparticles of Ag [27].

Fig. 5 shows the catalytic performance of Ag/c-Ga_2O_3 (CR_P) with controlled Ag loading for the photocatalytic conversion of CO_2 using H_2O. Bare c-Ga_2O_3 produced H_2 with an activity of 207.9 μmol h^{-1}, whereas CO was produced with an activity of just 0.3 μmol h^{-1} for the photocatalytic conversion of CO_2 by H_2O. When c-Ga_2O_3 was modified with 1 wt% Ag nanoparticles, the formation rate of CO increased to 115.1 μmol h^{-1} and that of H_2 was suppressed to 152.0 μmol h^{-1}. The selectivity toward CO evolution was 43%, similar to the results reported previously [12,14,17]. Interestingly, the selectivity toward CO evolution drastically increased to 93.4% at 4 wt% Ag nanoparticles. To the best of our knowledge, such a high selectivity toward CO evolution over bare Ga_2O_3 has not been reported when only Ag nanoparticles are used as the cocatalyst (generally selectivities of <50% have been achieved [12,14, 16–18]). Following this trend, the formation rate of H_2 was suppressed

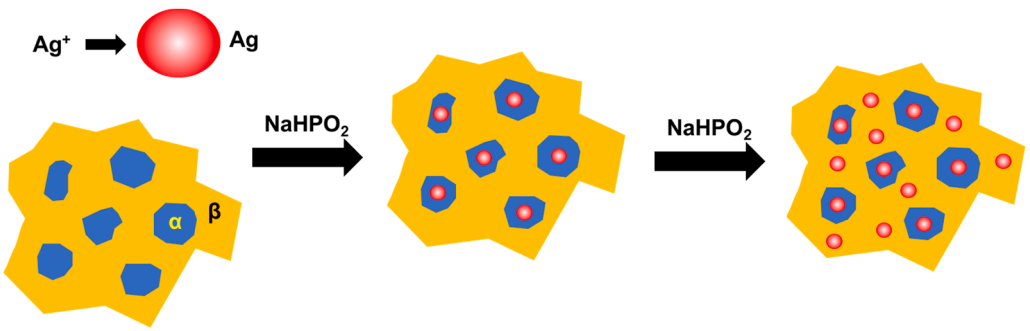

Scheme 1. The loading process of Ag nanoparticles on c-Ga_2O_3.

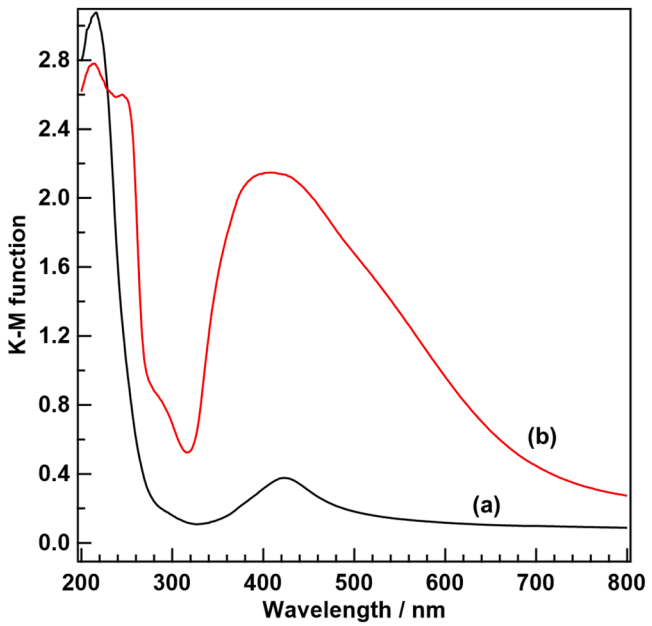

Fig. 6. Absorption spectra of (a) Ag/α-Ga_2O_3 (CR_P) and (b) Ag/β-Ga_2O_3 (CR_P) with 2 wt% Ag.

to 3.4 μmol h^{-1}, whereas that of CO remained stable at 2 wt% then decreased to 48.4 μmol h^{-1} at 3 wt%. Based on Figs. 3 and 4, the properties of the Ag nanoparticles loaded on c-Ga_2O_3, including their size and shape, remained unchanged with varying loadings. Thus, it could be concluded that the increased selectivity toward CO evolution was caused by the coverage ratio of Ag nanoparticles on the surfaces of c-Ga_2O_3. It has been reported that the α- and β-Ga_2O_3 phases in c-Ga_2O_3 exhibit positive [28] and negative [29] zeta potentials at pH values of the reactions in this work (about 6.8), respectively, whereas Ag nanoparticles exhibit negative zeta potential [30–32]. Therefore, we hold the opinion that the Ag nanoparticles were formed in the suspension solution first (Table S1) during chemical reduction and then selectively captured by the α phase of Ga_2O_3 owing to the Coulomb force. With saturated coverage of Ag nanoparticles on the α phase, Ag nanoparticles were then deposited on the surface of β phase of Ga_2O_3, as depicted in Scheme 1. In other words, Ag-loaded β-Ga_2O_3 showed high selectivity toward CO evolution for the photocatalytic conversion of CO_2 by H_2O.

3.2. *The influences of Ga_2O_3 phases*

Fig. 6 shows the UV–vis diffuse reflectance spectra of 2 wt% Ag-loaded α-Ga_2O_3 and β-Ga_2O_3 obtained via chemical reduction with NaH_2PO_2 (Fig. S3). The α-Ga_2O_3 and β-Ga_2O_3 showed absorption edges of 240 and 260 nm, respectively, corresponding to band gaps of 5.17 [33] and 4.77 eV [34], respectively. The Ag nanoparticles loaded in α-Ga_2O_3 exhibited an absorption band at 422 nm, whereas the peak was shifted to 410 nm for the Ag nanoparticles on β-Ga_2O_3. Fig. 7 compares the photocatalytic performances of Ag/α-Ga_2O_3 (CR_P) and Ag/β-Ga_2O_3 (CR_P) with 2 wt% Ag nanoparticle loading, including the product formation rate and selectivity toward CO evolution. Ag/α-Ga_2O_3 (CR_P) produced CO (25.3 μmol h^{-1}) with a selectivity of 33.4%. For Ag/β-Ga_2O_3 (CR_P), the CO formation rate reached 201.3 μmol h^{-1}, whereas that of H_2 was lowered to as much as 39.8 μmol h^{-1}. The selectivity of 83.5% over Ag/β-Ga_2O_3 (CR_P) conformed to the phenomenon observed in Fig. 5 and Scheme 1, and the β phase of Ga_2O_3 modified with Ag nanoparticles accounted for the high selectivity toward CO evolution. However, low loading amounts of Ag by chemical reduction of NaH_2PO_2 were not capable of producing CO in high selectivities over β-Ga_2O_3 (Fig. S4). Fig. 8 shows the photocatalytic performance of the optimized Ag-loaded α-Ga_2O_3 prepared via chemical reduction with NaH_2PO_2 for the photocatalytic conversion of CO_2 by H_2O. The H_2 formation rate was suppressed from 50.2 to 31.0 μmol h^{-1} as the loading of Ag nanoparticles increased from 2 to 5 wt%, whereas the CO evolution was largely unaffected (25.3 vs. 23.5 μmol h^{-1}). The H_2 evolution was further inhibited to 14.4 μmol h^{-1} when the loading of Ag nanoparticles reached 8 wt%, resulting in enhanced selectivity toward CO evolution (61.9%). Although a stronger suppression of H_2 evolution (12.4 μmol h^{-1}) was observed at higher Ag nanoparticle loading (10 wt%), the activity and selectivity for CO evolution also started to decline (16.4 μmol h^{-1}, 57.0%, respectively). This implies that the low selectivity for CO evolution over Ag-loaded α-Ga_2O_3 is likely caused by the properties of α-Ga_2O_3 rather than the Ag nanoparticle loading.

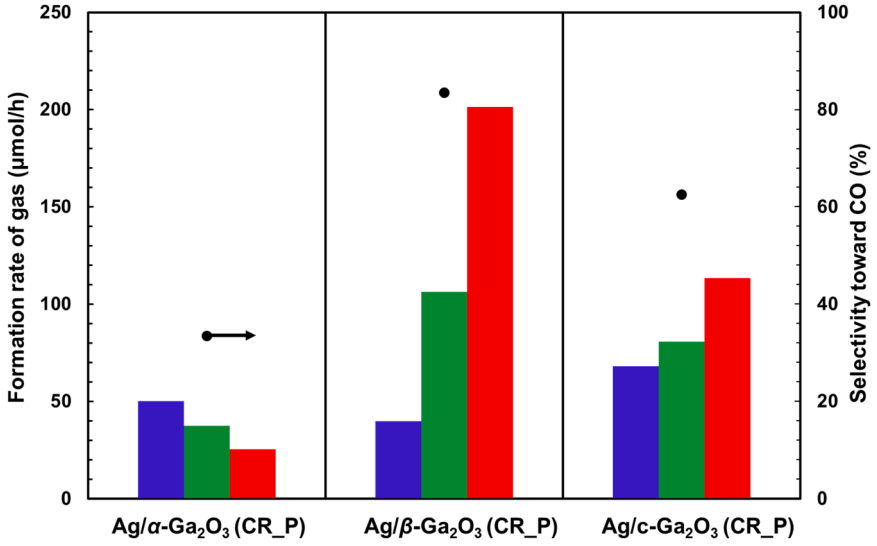

Fig. 7. Formation rates of H_2 (blue), O_2 (green), and CO (red) as well as selectivity toward CO evolution (black dots) for the photocatalytic conversion of CO_2 by H_2O over Ag/α-Ga_2O_3 (CR_P), Ag/β-Ga_2O_3 (CR_P) and Ag/c-Ga_2O_3 (CR_P). Photoirradiation time: 0.5 h; photocatalyst content: 0.25 g; Ag loading: 2 wt%; reaction solution: 1.0 L of a 0.1 M $NaHCO_3$ aqueous solution; CO_2 flow rate: 30 mL min^{-1}; light
Source: a 400 W high-pressure Hg lamp.

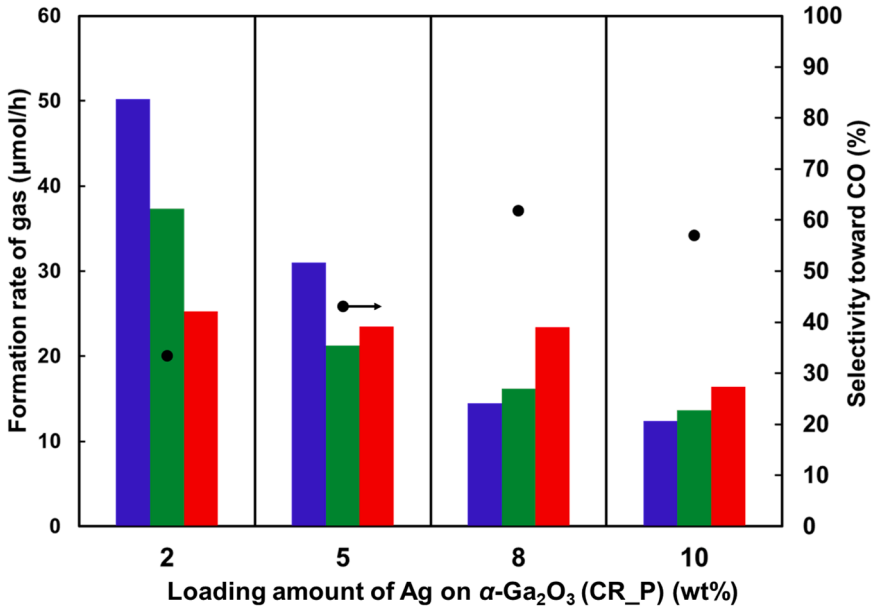

Fig. 8. Formation rates of H_2 (blue), O_2 (green), and CO (red) as well as selectivity toward CO evolution (black dots) for the photocatalytic conversion of CO_2 by H_2O over Ag/α-Ga_2O_3 (CR_P) with controlled loading of Ag nanoparticles. Photoirradiation time: 0.5 h; photocatalyst content: 0.25 g; reaction solution: 1.0 L of a 0.1 M $NaHCO_3$ aqueous solution; CO_2 flow rate: 30 mL min^{-1}; light
Source: a 400 W high-pressure Hg lamp.

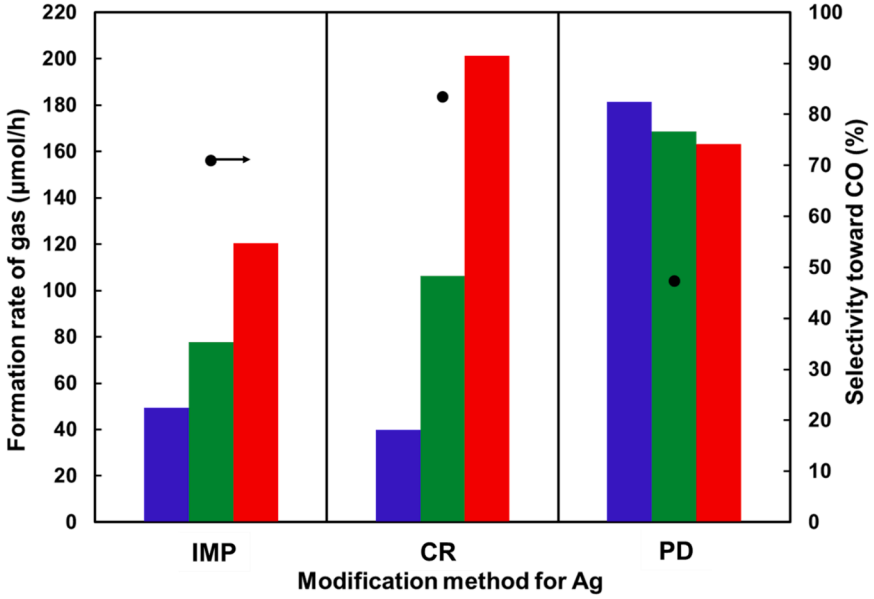

Fig. 9. Formation rates of H_2 (blue), O_2 (green), and CO (red) as well as selectivity toward CO evolution (black dots) for the photocatalytic conversion of CO_2 by H_2O over Ag/β-Ga_2O_3 loaded through impregnation (IM), chemical reduction (NaH_2PO_2), and photodeposition (PD) methods. Photoirradiation time: 0.5 h; photocatalyst content: 0.25 g; Ag loading: 2 wt%; reaction solution: 1.0 L of a 0.1 M $NaHCO_3$ aqueous solution; CO_2 flow rate: 30 mL min^{-1}; light
Source: a 400 W high-pressure Hg lamp.

3.3. Loading methods for Ag nanoparticles

Fig. 9 shows the photocatalytic performance of 2 wt% Ag-loaded β-Ga_2O_3 loaded by various methods, including chemical reduction, impregnation (IMP), and photodeposition (PD). Ag/β-Ga_2O_3 (IMP) showed 70.9% selectivity toward CO evolution with an activity of 120.4 μmol h^{-1}. In contrast, Ag/β-Ga_2O_3 (PD) produced CO with a selectivity of 47.4% over H_2, even though the activity reached 163.1 μmol h^{-1}. Fig. 10 shows the influence of the Ag loading on β-Ga_2O_3 through the photodeposition method on the photocatalytic conversion of CO_2 using H_2O. Similar to Ag/α-Ga_2O_3 (CR_P), the H_2 formation rates were significantly suppressed (181.4–74.1 and 52.3 μmol h^{-1}) over Ag/β-Ga_2O_3 (PD) when the Ag nanoparticle loadings were increased from 2 to 4 and 8 wt%, respectively. Interestingly, the CO evolution activity was not significantly affected with increased Ag nanoparticle loading (163.2, 191.1, and 187.6 μmol h^{-1} respectively). As a result, selectivity toward CO evolution was effectively increased from 47.4% to 78.2%.

3.4. The origin of high CO selectivity

The origin of the high selectivity toward CO evolution over Ag-loaded β-Ga_2O_3 for the photocatalytic conversion of CO_2 using H_2O was also investigated. Fig. 11 shows the dependence of Ag/β-Ga_2O_3 (CR_P) loading on selectivity toward CO evolution for the photocatalytic conversion of CO_2 using H_2O. 5 mg Ag/β-Ga_2O_3 (CR_P) produced H_2 and CO with activities of 11.4 and 7.3 μmol h^{-1} which could be normalized as 2280 and 1460 μmol g^{-1} h^{-1}, respectively. When the amount of catalyst was increased to 53 mg, CO evolution selectivity increased from

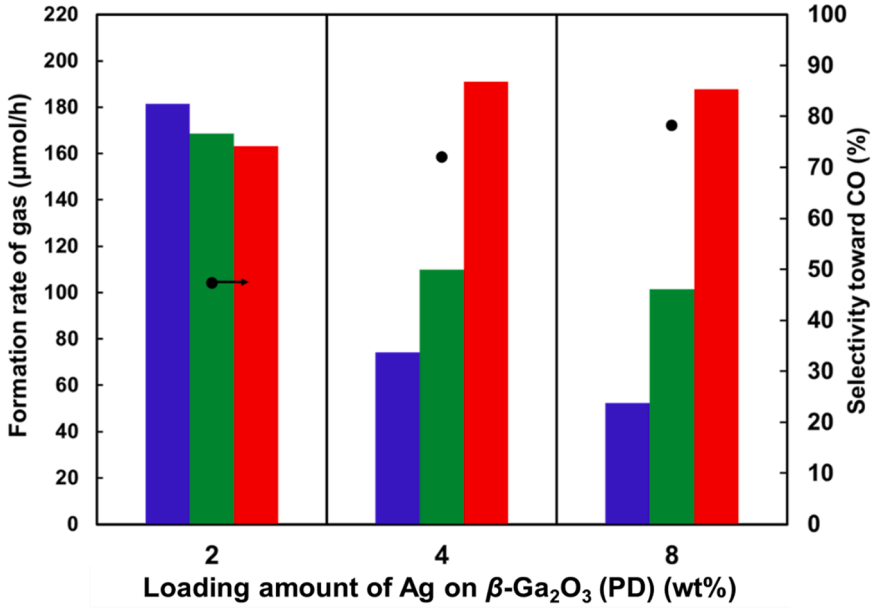

Fig. 10. Formation rates of H_2 (blue), O_2 (green), and CO (red) as well as selectivity toward CO evolution (black dots) for the photocatalytic conversion of CO_2 by H_2O over Ag/β-Ga_2O_3 (PD) with controlled loading of Ag nanoparticles. Photoirradiation time: 0.5 h; photocatalyst content: 0.25 g; reaction solution: 1.0 L of a 0.1 M $NaHCO_3$ aqueous solution; CO_2 flow rate: 30 mL min^{-1}; light
Source: a 400 W high-pressure Hg lamp.

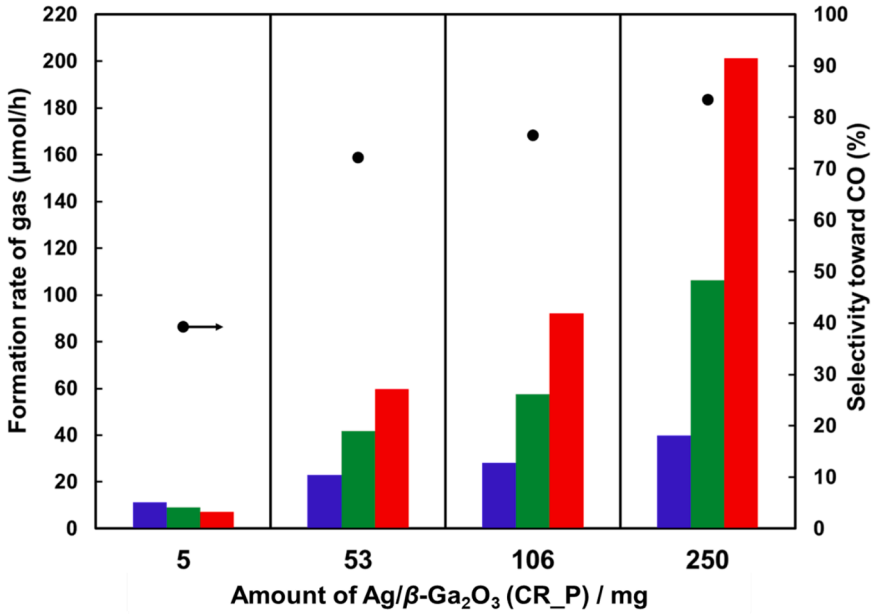

Fig. 11. Formation rates of H_2 (blue), O_2 (green), and CO (red) as well as selectivity toward CO evolution (black dots) for the photocatalytic conversion of CO_2 by H_2O over different amounts of Ag/β-Ga_2O_3 (CR_P). Photoirradiation time: 0.5 h for each amount; Ag loading: 2 wt%; reaction solution: 1.0 L of a 0.1 M $NaHCO_3$ aqueous solution; CO_2 flow rate: 30 mL min^{-1}; light
Source: a 400 W high-pressure Hg lamp.

39.2% to 72.1% and the normalized activities for H_2 and CO were 433.9 and 1124.5 μmol g^{-1} h^{-1}, respectively. At a catalyst loading of 106 mg, the H_2 formation rate decreased to 266.0 μmol g^{-1} h^{-1}, whereas 867.9 μmol g^{-1} h^{-1} for CO, respectively. At 250 mg, the H_2 formation rate dropped to 159.2 μmol g^{-1} h^{-1} but that of CO (805.2 μmol g^{-1} h^{-1}) remained largely unchanged. The normalized activities imply that H_2 evolution was drastically suppressed with increasing Ag/β-Ga_2O_3 (CR_P) loading, whereas CO was negligibly affected. Moreover, Fig. 12 shows the dependence of the 8 wt% Ag/β-Ga_2O_3 (PD) photocatalyst loading on the CO evolution selectivity for the photocatalytic conversion of CO_2 by H_2O. The loading of 5 mg Ag/β-Ga_2O_3 (PD) produced H_2 with an activity of 14.8 μmol h^{-1}, greatly exceeding that of CO (3.3 μmol h^{-1}). When the amount of photocatalyst was increased to 51 mg, the H_2 and CO formation rates increased 38.5 and 51.9 μmol h^{-1}, respectively. Correspondingly, the selectivity for CO evolution increased from 18.2% to 57.4%. Higher amounts of Ag/β-Ga_2O_3 (PD) (106 and 250 mg) exhibited limited effects on the evolution of H_2 (45.5 and 52.3 μmol h^{-1} respectively), whereas the CO formation rates increased by 2.1 and 3.6 times (107.9 and 187.6 μmol h^{-1}), respectively. Consequently, the selectivity toward CO evolution increased to 78.2% at 250 mg.

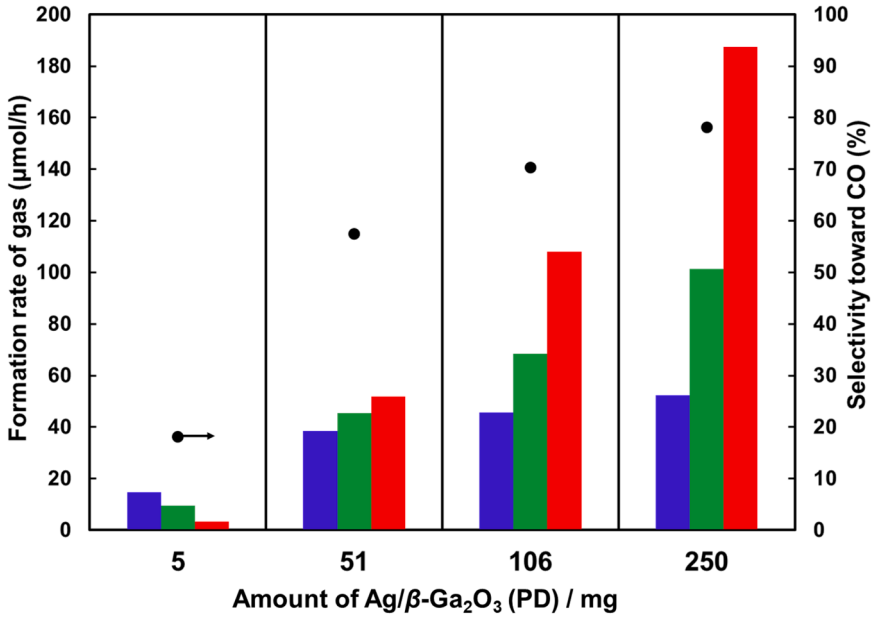

Fig. 12. Formation rates of H_2 (blue), O_2 (green), and CO (red) as well as selectivity toward CO evolution (black dots) for the photocatalytic conversion of CO_2 by H_2O over different amounts of Ag/β-Ga_2O_3 (PD). Photoirradiation time: 0.5 h for each amount; Ag loading: 8 wt%; reaction solution: 1.0 L of a 0.1 M $NaHCO_3$ aqueous solution; CO_2 flow rate: 30 mL min^{-1}; light
Source: a 400 W high-pressure Hg lamp.

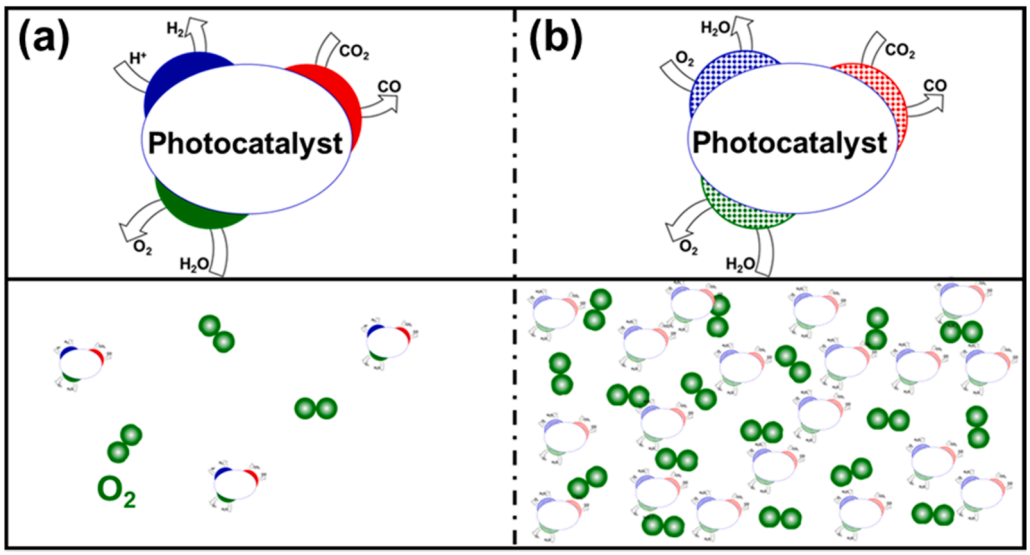

Scheme 2. Dependence of CO evolution selectivity on the amount of photocatalyst used in the photocatalytic conversion of CO_2 by H_2O. (a) low and (b) high amounts of photocatalysts, respectively.: Active sites for H_2 (blue), CO (red) and O_2 (green) evolutions.

As shown in Fig. 5, 0.25 g bare Ga_2O_3 failed to produce CO with high selectivity during the photocatalytic conversion of CO_2 by H_2O, indicating that Ag nanoparticles are essential for achieving high selectivity. However, the dependence of CO selectivity on the amount of Ag-loaded β-Ga_2O_3 implied that the Ag nanoparticles were not the sole contributor. Scheme 2 depicts the proposed mechanism by which Ag-loaded β-Ga_2O_3 photocatalysts obtained from proper synthesis methods exhibit high selectivity toward CO evolution in the photocatalytic conversion of CO_2 by H_2O. Undoubtedly, higher amounts of photocatalysts increase the number of photocatalyst particles, which would correspond to increased O_2 evolution from H_2O (Scheme 2(b)). A high concentration of aqueous O_2 and a large number of suspended photocatalyst particles would inevitably allow for sufficient contact between O_2 and the particles. Because the redox potential of O_2 is much lower than that of protons and the reduction of O_2 consumes large amounts of protons, O_2 would selectively poison the active sites for H_2 evolution. Finally, O_2 reduction at the sites of H_2 evolution and H_2O oxidation at the sites of O_2 evolution forms a dynamic loop, resulting selective suppression of H_2 evolution relative to CO. Note that the reverse reaction of H_2 and O_2 into H_2O was difficult to proceed on the surfaces of Ag-loaded Ga_2O_3 (Fig. S5). However, the O_2 and photocatalyst particles failed to sufficiently contact each other because of the low O_2 and particle concentrations when the amount of photocatalyst was kept low levels such as 5.0 mg (Scheme 2 (a)). On the other hand, it was expected that O_2 molecules were difficult to adsorb on the surfaces of photocatalyst particles at low concentration of O_2 in the solutions because of the adsorption equilibrium. This would further suppress ORR proceeded on the surfaces of photocatalysts. As a result, the active sites for H_2 evolution were not poisoned by O_2

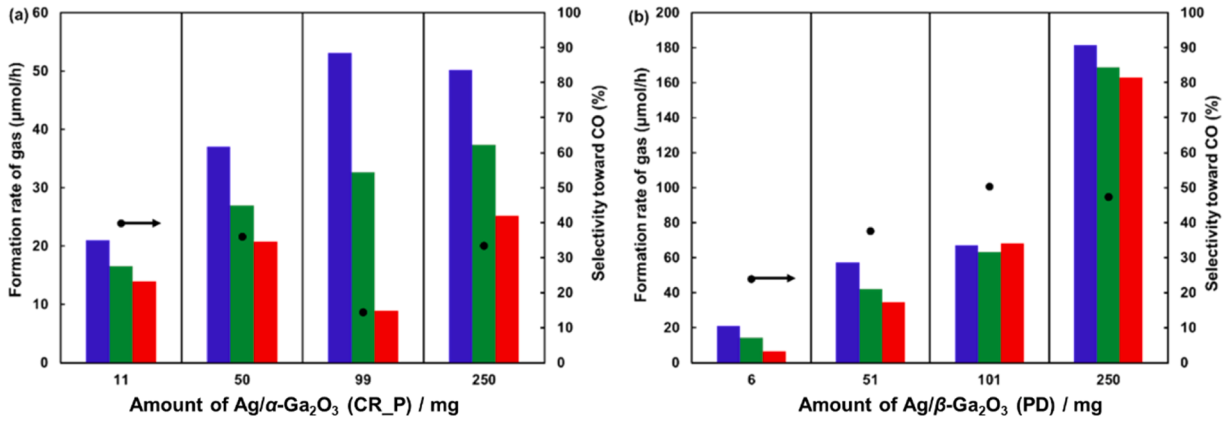

Fig. 13. Formation rates of H_2 (blue), O_2 (green), and CO (red) as well as selectivity toward CO evolution (black dots) for the photocatalytic conversion of CO_2 by H_2O over different amounts of (a) Ag/α-Ga_2O_3 (CR_P) and (b) Ag/β-Ga_2O_3 (PD). Photoirradiation time: 0.5 h for each amount; Ag loading: 2 wt%; reaction solution: 1.0 L of a 0.1 M $NaHCO_3$ aqueous solution; CO_2 flow rate: 30 mL min^{-1}; light Source: a 400 W high-pressure Hg lamp.

reduction. In this case, CO is produced with poor selectivity from the photocatalytic conversion of CO_2 by H_2O. In other words, the high selectivity for CO evolution was not caused by the Ag nanoparticles alone, but by the synergistic effects between the Ag nanoparticles and O_2 poisoning of the active sites for H_2 evolution.

To confirm the proposed mechanism, the dependence of CO evolution selectivity on the amount of photocatalyst Ag/α-Ga_2O_3 (CR_P) (2 wt %) and Ag/β-Ga_2O_3 (PD) (2 wt%) was examined, as presented in Fig. 13. From Fig. 13(a), 11 mg of Ag/α-Ga_2O_3 (CR_P) prepared via chemical reduction method produced CO with an activity of 13.9 μmol h^{-1} and selectivity of 39.8%. The selectivity toward CO during the photocatalytic conversion of CO_2 by H_2O was not promoted (33.5%), producing CO and H_2 at 25.3 and 50.2 μmol h^{-1}, respectively, even when 250 mg of Ag/α-Ga_2O_3 (CR_P) was used. This indicates that the evolution of H_2 over Ag/α-Ga_2O_3 (CR_P) was not selectively suppressed with increasing amounts of photocatalysts. A similar trend was also observed for Ag/β-Ga_2O_3 (PD), as shown in Fig. 13(b), where 5.6 mg Ag/β-Ga_2O_3 (PD) showed a selectivity of 23.9% toward CO evolution and CO and H_2 formation rates were 6.6 and 21.1 μmol h^{-1}, respectively. The selectivity increased to 50.4% with formation rates of 68.0 and 67.0 μmol h^{-1} for CO and H_2, respectively, when 101 mg of photocatalyst was used. However, the selectivity (47.4%) for CO evolution did not further increase with higher photocatalyst loadings (250 mg), even though the formation rates of CO (163.1 μmol h^{-1}) and H_2 (181.4 μmol h^{-1}) significantly increased. The discrepancy between 2 and 8 wt% Ag loading by photodeposition method on β-Ga_2O_3 was probably caused by the sizes of Ag nanoparticles (Fig. S6).

4. Conclusion

Herein, the amounts and loading methods of Ag nanoparticles, including chemical reduction, photodeposition, and impregnation, were optimized on commercial Ga_2O_3 (composite of α-Ga_2O_3 and β-Ga_2O_3) as well as pure α-Ga_2O_3 and β-Ga_2O_3 photocatalysts for the photocatalytic conversion of CO_2 using H_2O as the electron donor. High selectivity towards CO evolution was achieved for this reaction when the proper catalyst amounts and loading methods were controlled using β-Ga_2O_3 as a starting material. After optimizing the amount of Ag-loaded β-Ga_2O_3 catalyst, the high CO evolution selectivity was determined to largely depend on the amount of the photocatalyst present. A large amount of Ag-loaded β-Ga_2O_3 enhanced active site poisoning for the evolution of H_2 via O_2 reduction, indirectly promoting selectivity toward CO evolution.

CRediT authorship contribution statement

Xuanwen Xu: Designing and carrying out experiments; Carrying out characterizations; Processing data; Writing - original draft. Tsunehiro Tanaka: Supervision; Reviewing the manuscript. Kentaro Teramura: Supervision; Writing - review & editing.

Declaration of Competing Interest

The authors declare that they have no known competing financial interests or personal relationships that could have appeared to influence the work reported in this paper.

Data availability

Data will be made available on request.

Acknowledgements

This research was partially supported by the Program for Elements Strategy Initiative for Catalysts and Batteries (ESICB) commissioned by the Ministry of Education, Culture, Sports, Science, and Technology (MEXT) of Japan. This work was also supported by JSPS KAKENHI (Grant Number 21H01716), a Research Grant against Global Warming of the Ichimura Foundation for New Technology, and the CASIO SCIENCE PROMOTION FOUNDATION. Xuanwen Xu thanks the State Scholarship of the China Scholarship Council, affiliated with the Ministry of Education of the People's Republic of China. Prof. Hisao Yoshida in Kyoto University provided assistant in XRF measurements.

Appendix A. Supporting information

Supplementary data associated with this article can be found in the online version at doi:10.1016/j.apcatb.2022.122027.

References

[1] C. Oertel, J. Matschullat, K. Zurba, F. Zimmermann, S. Erasmi, Chem. der Erde 76 (2016) 327–352.
[2] W.D. Nordhaus, Am. Econ. Rev. 96 (2) (2006) 31–34.
[3] N.L. Panwar, S.C. Kaushik, S. Kothari, Renew. Sustain. Energy Rev. 15 (2011) 1513–1524.
[4] N. Kannan, D. Vakeesan, Renew. Sustain. Energy Rev. 62 (2016) 1092–1105.
[5] A. Wang, J. Zhao, M.A. Appl, Phys. Lett. 57 (1990) 602–604.
[6] B. Parida, S. Iniyan, R. Goic, Renew. Sustain. Energy Rev. 15 (2011) 1625–1636.
[7] I.L. Granone, F. Sieland, N. Zheng, R. Dillert, D.W. Bahnemann, Green. Chem. 20 (2018) 1169–1192.

[8] Q. Wang, K. Domen, Chem. Rev. 120 (2) (2020) 919–985.
[9] W. Tu, Y. Zhou, Z. Zou, Adv. Mater. 6 (2014) 4607–4626.
[10] H. Nakanishi, K. Iizuka, T. Takayama, A. Iwase, A. Kudo, ChemSusChem 10 (2017) 112–118.
[11] A. Anzai, N. Fukuo, A. Yamamoto, H. Yoshida, Catal. Commun. 100 (2017) 134–138.
[12] R. Pang, K. Teramura, H. Tatsumi, H. Asakura, S. Hosokawa, T. Tanaka, Chem. Commun. 54 (2018) 1053–1056.
[13] Z. Wang, K. Teramura, S. Hosokawa, T. Tanaka, J. Mater. Chem. A 3 (2015) 11313–11319.
[14] Y. Kawaguchi, M. Akatsuka, M. Yamamoto, K. Yoshida, A. Ozawa, Y. Kato, T. Yoshida, J. Photochem. Photobiol. A Chem. 358 (2018) 459–464.
[15] Q. Li, Y. Zhang, L. Zhang, J. Xia, X. Liu, L. Hu, F. Wang, X. Chu, P. Zhao, J. Yin, D. Yang, Catal. Commun. 120 (2019) 23–27.
[16] Z. Huang, K. Teramura, H. Asakura, S. Hosokawa, T. Tanaka, J. Mater. Chem. A 5 (2017) 19351–19357.
[17] H. Tatsumi, K. Teramura, Z. Huang, Z. Wang, H. Asakura, S. Hosokawa, T. Tanaka, Langmuir 33 (2017) 13929–13935.
[18] S. Iguchi, Y. Hasegawa, K. Teramura, S. Kidera, S. Kikkawa, S. Hosokawa, H. Asakura, T. Tanaka, Sustain. Energy Fuels 1 (2017) 1740–1747.
[19] K. Teramura, Z. Wang, S. Hosokawa, Y. Sakata, T. Tanaka, Chem. A Eur. J. 20 (2014) 9906–9909.
[20] Z. Wang, K. Teramura, Z. Huang, S. Hosokawa, Y. Sakata, T. Tanaka, Catal. Sci. Technol. 6 (2016) 1025–1032.
[21] T. Soltani, A. Yamamoto, S.P. Singh, A. Anzai, E. Fudo, A. Tanaka, H. Kominami, H. Yoshida, ACS Appl. Energy Mater. 4 (2021) 6500–6510.
[22] Z. Jiang, G. Wen, Y. Luo, X. Zhang, Q. Liu, A. Liang, Sci. Rep. 4 (2014) 5323.
[23] M. Luo, H. Huang, S. Choi, C. Zhang, R.R.D. Silva, H.C. Peng, Z. Yuan, J. Liu, Z. He, Y. Xia, ACS Nano 9 (2015) 10523–10532.
[24] N. Fitria, M. Sujak, D. Djuhana, IOP Conf. Ser.: Mater. Sci. Eng. 763 (2020), 012062.
[25] B. Chen, X. Jiao, D. Chen, Cryst. Growth Des. 10 (2010) 3378–3386.
[26] J. Zhang, H. Liu, Z. Wang, N. Ming, Adv. Funct. Mater. 17 (2007) 3295–3303.
[27] W. Rechberger, A. Hohenau, A. Leitner, J.R. Krenn, B. Lamprecht, F.R. Aussenegg, Opt. Commun. 220 (2003) 137–141.
[28] J.N. Díaz de León, Appl. Catal. B Environ. 181 (2016) 524–533.
[29] S. Mandal, K. Arts, H.C.M. Knoops, J.A. Cuenca, G.M. Klemencic, O.A. Williams, Carbon 181 (2021) 79–86.
[30] S. Kokura, O. Handa, T. Takagi, T. Ishikawa, Y. Naito, T. Yoshikawa, Nanomed.: NBM 6 (2010) 570–574.
[31] S. Magdassi, A. Bassa, Y. Vinetsky, A. Kamyshny, Chem. Mater. 15 (2003) 2208–2217.
[32] L. Xu, G. Han, J. Hu, Y. He, J. Pan, Y. Li, J. Xiang, Phys. Chem. Chem. Phys. 11 (2009) 6490–6497.
[33] A. Barthel, J. Roberts, M. Napari, M. Frentrup, T. Huq, A. Kovacs, R. Oliver, P. Chalker, T. Sajavaara, F. Massabuau, Micromachines 11 (2020) 1–11.
[34] M. Mohamed, I. Unger, C. Janowitz, R. Manzke, Z. Galazka, R. Uecker, R. Fornari, J. Phys. Conf. Ser. 286 (2011), 012027.